GEOPHYSICS, VOL. 71, NO. 6 (NOVEMBER-DECEMBER 2006); P. W45–W58, 11 FIGS.
10.1190/1.2360212

DOI:10.1190/1.2360212

Effective elasticity of fractured rocks: A snapshot of the work in progress

Vladimir Grechka[1] and Mark Kachanov[2]

ABSTRACT

Exploration and development of naturally fractured reservoirs rely on understanding and interpretation of certain signatures associated with seismic waves propagating through cracked rocks. This understanding comes primarily from the effective media theories that predict an overall elastic behavior of a solid containing many inhomogeneities (cracks, in particular) whose sizes are too small to be "seen" individually by the waves. To model seismic responses of fractured formations, a geophysicist typically has a choice between the effective media schemes of Hudson and Schoenberg. While the two predictions usually deviate slightly for liquid-filled cracks, the differences are significant when the fractures are dry. Explaining the origin of these differences and selecting a more accurate scheme is the first goal of this tutorial. Our second, more challenging task, is to prove that simply adding the compliance contributions of cracks as if they were isolated and noninteracting remains sufficiently accurate even for fractures that grossly violate the basic theoretical assumption, of penny-shaped cracks. Real fractures have notoriously irregular shapes, might be partially closed, and often form interconnected networks. Yet, these details of fracture microgeometry turn out to be unimportant for the effective elasticity given a typical noise level in seismic data. No closed-form theory exists for irregular fracture shapes. However, take into account finite-element simulations on so-called digital rocks demonstrate which features of the crack geometry have to be taken into account because they influence propagation of long (compared to the size of fractures) seismic waves and which features can be ignored.

INTRODUCTION

Continuous depletion of conventional clastic hydrocarbon fields makes naturally fractured reservoirs an important target for the oil industry. Production of these reservoirs, whose matrix permeability often lies in the microdarcy range, is controlled by the networks of natural cracks that provide highly permeable conduits for fluid flow. Given the importance of fractures for production, such reservoir development is greatly aided by any information about the cracks obtained from seismic data. Although fractures in the subsurface usually come in all sizes, here we restrict our discussion to the cracks whose sizes are much smaller than the seismic wavelengths used in a particular application. Seismic waves cannot "see" such cracks individually. Instead, the measured wave signatures are governed by certain average characteristics of multiple fractures.

Analysis of these signatures reveals that a low-frequency seismic response of a fractured rock can be reproduced in a properly selected homogeneous solid. This fact justifies the use of the so-called effective media or homogenization theories that aim at replacing a microheterogeneous material with a homogeneous one that is equivalent to the former in the regime of static deformation. The overall properties of cracked solids are of obvious relevance to many materials science problems, and development of the effective media theories began there with a seminal paper of Eshelby (1957), which discusses a single ellipsoidal inclusion in an otherwise homogeneous elastic solid, and a paper of Bristow (1960) explicitly devoted to thin cracks. The first rock physics applications of the effective media theories are attributable to Walsh (1965a, b) for rocks with dry cracks and to O'Connell and Budiansky (1974) for cracks filled with a liquid. All the above mentioned and numerous other authors describe fractures as compliant inclusions in a relatively stiff unfractured matrix. While other possibilities have been exploited also (for instance, one can treat cracks as contacts of rough surfaces or as infinite thin soft layers with occasional asperities), this tutorial is exclusively devoted to the inclusion model of cracks as the most common.

It took longer for the exploration community to address these issues, and then papers by Hudson (1980) and Schoenberg (1980) appeared. Even though substantial progress in effective media theories has been made both in materials and earth sciences since 1980, today's typical geophysicist, examining seismic data acquired over a fractured reservoir, still chooses between the Hudson's theory and the linear slip theory of Schoenberg. Such a choice is not straightfor-

Manuscript received by the Editor March 9, 2006; revised manuscript received June 1, 2006; published online November 3, 2006.
[1]Shell International Exploration and Production, Inc., 3737 Bellaire Blvd., P.O. Box 481, Houston, Texas 77001. E-mail: vladimir.grechka@shell.com.
[2]Tufts University, Department of Mechanical Engineering, Medford, Massachusetts 02155. E-mail: mark.kachanov@tufts.edu.

ward, especially for dry cracks where Hudson's and Schoenberg's theories give substantially different predictions. People seem to prefer Hudson's theory because it links the effective properties to density of circular cracks. In contrast, the linear slip theory of Schoenberg (1980) operates with the quantities — the excess fracture compliances — that usually play the role of adjustable parameters and do not have to be expressed through any geometric characteristics of the fractures. Even after the relations between the geometry of penny-shaped cracks and the fracture compliances have been established (Schoenberg and Douma, 1988), proponents of the linear slip theory still refrain from using them (Schoenberg and Sayers, 1995; Sayers, 2002a, b; Schoenberg 2002), preserving the potential generality of their approach and sacrificing its explicit connections to the crack microstructure.

In our view, this is unfortunate because the accuracy of the linear slip theory turns out to be superior to that of Hudson's. The first part of our tutorial demonstrates that. Specifically, we explain why the stiffness-based Hudson's theory is bound to be less accurate than the compliance-based Schoenberg's. While we rely on basic theoretical findings made in solid mechanics, we support our statements with finite-element simulations on the so-called digital rocks.

Being free from assumptions inherent for all existing effective media theories, direct computational studies provide an independent verification of theoretical predictions. Perhaps more importantly, finite-element simulations allow us to examine realistic fracture models that violate the conventional assumptions. These models contain irregularly shaped cracks that can be partially closed, might intersect each other, and form interconnected networks. The second part of our tutorial discusses such fracture arrays. Quite remarkably, we show that the linear slip theory, supplemented by the well-understood behavior of isolated penny-shaped cracks, satisfactorily predicts the effective elasticity of all our models. One of those predictions (made by Kachanov, 1980) is especially counterintuitive. It states that the symmetry of effective media resulting from isolated dry circular fractures, embedded in an otherwise isotropic host rock, is almost orthorhombic (or orthotropic) regardless of the number of fracture sets and their orientations. We verify this prediction numerically both for dry and liquid-filled fractures that have circular and noncircular shapes. This and other results discussed below lead to the most important message of our tutorial: *Virtually all conclusions drawn for isolated, penny-shaped cracks remain valid for planar, irregular, possibly intersecting fractures that might form interconnected networks*.

Most of our tutorial is devoted to dry cracks because they influence the overall elasticity to the greatest extent. Liquid infill of fractures causes stiffening of the effective properties (O'Connell and Budiansky, 1974; Budiansky and O'Connell, 1976; Hudson, 1981; Shafiro and Kachanov, 1997) and significantly reduces all crack-related signatures. Consequently, many conventional theories yield comparable predictions for liquid-filled fractures. We intentionally refrain from discussing the fractures in porous rocks where fluid flow between the pores and fractures is important. Analysis of such media can be found in Thomsen (1995), Cardona (2002), and Gurevich (2003).

We begin with elementary considerations of the accuracy of the most frequently used Hudson's (1980) theory and then describe the basics of effective elasticity of fractured media. Next, we compare various theoretical predictions with direct computational simulations and, finally, give an overview of literature on the effective elastic properties of solids with cracks (Appendix A).

ON THE ACCURACY OF HUDSON'S THEORY

There is little doubt that Hudson's (1980) effective media theory is the most popular in exploration geophysics. Despite such popularity and perhaps quite unexpectedly, its accuracy is inferior to many other theories. Our reason relies on certain obvious features of the effective stiffness tensor

$$\mathbf{c}_e \equiv \{c_{e,ij}\}, \quad (i,j = 1, \ldots ,6). \tag{1}$$

Here we employ Voigt notation to represent the fourth-rank tensor c_e as a symmetric 6×6 matrix. We denote the stiffness tensor of isotropic background rock with $\mathbf{c}_b$.

To examine the influence of fractures on $\mathbf{c}_e$, we need a measure for the amount of fracturing. This measure is known as the crack density, e, so that $\mathbf{c}_e = \mathbf{c}_e(e)$ and

$$\mathbf{c}_e(0) = \mathbf{c}_b. \tag{2}$$

We now focus our attention on the effective stiffness component $c_{e,11}$ that controls the P-wave velocity across parallel cracks whose normals are directed along the $\mathbf{x}_1$-axis of a chosen coordinate frame. The cracks reduce the stiffness; therefore, $c_{e,11}(e)$ is a monotonically decreasing function of e.

Following Hudson (1980), we expand $c_{e,11}(e)$ in the power series:

$$c_{e,11}(e) = c_{b,11} + \left.\frac{dc_{e,11}}{de}\right|_{e=0} e + \frac{1}{2}\left.\frac{d^2c_{e,11}}{de^2}\right|_{e=0} e^2 + \ldots . \tag{3}$$

Because $c_{e,11}(e)$ decreases with crack density and the linear term dominates at sufficiently small e,

$$\left.\frac{dc_{e,11}(e)}{de}\right|_{e=0} < 0. \tag{4}$$

Thus, truncating series 3 after the liner term in accordance with the first-order Hudson's (1980) approximation inevitably results in incorrect negative $c_{e,11}$ at some crack density e. Hudson's (1980) second-order theory yields a positive coefficient of the quadratic term in expansion 3. Therefore, $c_{e,11}(e)$ begins to increase at some point, also exhibiting an unphysical behavior. We discuss Hudson's predictions in more detail below and illustrate them in Figure 1.

It is instructive to compare Hudson's theory with the noninteraction approximation (e.g., Bristow, 1960) that ignores elastic interactions between the cracks and sums up their contributions to the effective compliance, the quantity reciprocal to the effective stiffness. The noninteraction result, linear in the crack density, can be rewritten in the stiffnesses as

$$c^{\mathrm{NIA}}_{e,11}(e) = \frac{c_{b,11}}{1 + \kappa_{11}e}, \tag{5}$$

where κ_{11} is a positive dimensionless coefficient. Note that $c^{\mathrm{NIA}}_{e,11}(e)$ is a positive, monotonically decreasing function of e as it should be.

Linearization of the noninteraction approximation 5 in e (the so-called dilute limit) recovers expansion 3 up to its linear term, but such a linearization results in a significant reduction of the accuracy of equation 5 (Kachanov, 1992; 1993) and should be avoided.

BASIC CONCEPTS AND THE NONINTERACTION APPROXIMATION

The effective stiffness $\mathbf{c}_e$ of a heterogeneous (for instance, fractured) rock enters Hooke's law written for the representative volume V:

$$\boldsymbol{\tau} = \mathbf{c}_e : \boldsymbol{\varepsilon}. \tag{6}$$

Here $\boldsymbol{\tau}$ and $\boldsymbol{\varepsilon}$ are the stress and strain tensors, respectively, averaged over V; $\mathbf{c}_e$ is the effective (that is, constant in V) stiffness tensor, and the colon denotes a double-dot product. Alternatively, we can use the effective compliance tensor,

$$\mathbf{s}_e = \mathbf{c}_e^{-1}, \tag{7}$$

and write Hooke's law in an equivalent form

$$\boldsymbol{\varepsilon} = \mathbf{s}_e : \boldsymbol{\tau}. \tag{8}$$

Formulation 8 turns out to be more appropriate for fractured solids because cracks are the sources of extra strains. This can be made explicit by splitting $\mathbf{s}_e$ into the background $\mathbf{s}_b$ and the fracture-contribution, $\Delta\boldsymbol{s}$, terms,

$$\mathbf{s}_e \equiv \mathbf{s}_b + \Delta\mathbf{s}, \tag{9}$$

and rewriting equation 8 as

$$\boldsymbol{\varepsilon} = \mathbf{s}_b : \boldsymbol{\tau} + \Delta\mathbf{s} : \boldsymbol{\tau} = \mathbf{s}_b : \boldsymbol{\tau} + \Delta\boldsymbol{\varepsilon}, \tag{10}$$

where $\Delta\boldsymbol{\varepsilon} = \Delta\mathbf{s} : \boldsymbol{\tau}$ is the extra strain resulting from cracks. The strain $\Delta\boldsymbol{\varepsilon}$ can be expressed in terms of physically transparent quantities — the displacement discontinuities across crack areas (Vavakin and Salganik, 1975):

$$\Delta\boldsymbol{\varepsilon} = \frac{1}{2V}\sum_k \int_{A^{(k)}} (\mathbf{n}[\mathbf{u}] + [\mathbf{u}]\mathbf{n})^{(k)} dA^{(k)}. \tag{11}$$

Here $[\mathbf{u}] = \mathbf{u}^+ - \mathbf{u}^-$ is the vector of displacement discontinuity across a point at the crack surface A; $\mathbf{n}$ is the unit normal to the fracture face, and the sum is taken with respect to all cracks k in volume V.

Let us make our first simplification and assume that the cracks are flat. Then $\mathbf{n}$ is constant at A, and the previous equation becomes

$$\Delta\boldsymbol{\varepsilon} = \frac{1}{2V}\sum_k [(\mathbf{nb} + \mathbf{bn})A]^{(k)}, \tag{12}$$

where $\mathbf{b} = \langle[\mathbf{u}]\rangle$ is the displacement-discontinuity vector averaged over the crack area. Obtaining the effective compliances is thus reduced to finding vector $\mathbf{b}$.

The second simplification rests on an important assumption that interactions in the stress fields of different cracks can be ignored (the so-called noninteraction approximation), so that each crack senses the far-field stress $\boldsymbol{\tau}$. As a consequence, $\mathbf{b}$ is calculated for isolated fractures in terms of the symmetric, second-rank excess fracture compliance tensor $\mathbf{Z}$ (Schoenberg, 1980; Kachanov, 1992). The latter relates vector $\mathbf{b}$ to the uniform traction $\mathbf{n}\cdot\boldsymbol{\tau}$ induced at the crack face by the remotely applied stress,

$$\mathbf{b} = \mathbf{n} \cdot \boldsymbol{\tau} \cdot \mathbf{Z}. \tag{13}$$

The eigenvectors of symmetric, positive-definite tensor $\mathbf{Z}$ are the principal directions of compliance of a flat crack that has an arbitrary shape. If host material is isotropic, one of the eigenvectors coincides with the crack normal $\mathbf{n}$, while the other two, $\mathbf{r}$ and $\mathbf{t}$, lie in the crack plane (Sevostianov and Kachanov, 2002):

$$\mathbf{Z} = Z_N\mathbf{nn} + Z_R\mathbf{rr} + Z_T\mathbf{tt}. \tag{14}$$

The eigenvalue Z_N is called the normal crack compliance, and Z_R, Z_T are the shear compliances.

While $\mathbf{Z}$-tensor was originally introduced by Schoenberg (1980), components of $\mathbf{Z}$ for circular and elliptic cracks can be extracted from an earlier paper of Budiansky and O'Connell (1976); Kachanov (1992; 1993) gave their explicit expressions. Sevostianov and Kachanov (2002) obtained estimates of Z_N for several irregular crack geometries, and Grechka et al. (2006) described a numerical approach for computing $\mathbf{Z}$-tensors for arbitrary fracture shapes.

Elastic potential

It is instructive to reformulate the problem of obtaining the effective properties in terms of the elastic energy stored in a solid or the elastic potential:

$$f(\boldsymbol{\tau}) = \frac{1}{2}\boldsymbol{\tau} : \boldsymbol{\varepsilon}. \tag{15}$$

Definitions 8 and 15 make it possible to find $\mathbf{s}_e$ by differentiation:

$$\mathbf{s}_e : \boldsymbol{\tau} = \frac{\partial f(\boldsymbol{\tau})}{\partial \boldsymbol{\tau}}. \tag{16}$$

While being equivalent to the compliance formulation, the description of the effective properties, in terms of the elastic potential, has one significant advantage: The structure of f identifies the proper tensorial crack-density parameters that govern the overall elasticity. As implied by equation 10, the potential f is a sum

$$f = f_b + \Delta f, \tag{17}$$

where (e.g., Landau and Lifshitz, 1998)

$$f_b(\boldsymbol{\tau}) = \frac{1 + \nu_b}{2E_b}\boldsymbol{\tau} : \boldsymbol{\tau} - \frac{\nu_b}{2E_b}[\mathrm{tr}(\boldsymbol{\tau})]^2 \tag{18}$$

is the potential of the uncracked solid, Δf is its change resulting from the presence of cracks, E_b and ν_b are the Young's modulus and Poisson's ratio of the background, and $\mathrm{tr}(\boldsymbol{\tau})$ denotes the trace of tensor $\boldsymbol{\tau}$. The change Δf can be written in terms of tensors $\mathbf{Z}$ of the cracks residing in representative volume V:

$$\Delta f = \boldsymbol{\tau} : \left[\frac{1}{2V}\sum_k (\mathbf{nZn}A)^{(k)}\right] : \boldsymbol{\tau}. \tag{19}$$

Scalar cracks

The simplest and yet most important case is when $\mathbf{Z}$-tensor is proportional — exactly or approximately — to the unit tensor:

$$\mathbf{Z} = \mathbb{Z}\mathbf{I}, \tag{20}$$

where $\mathbb{Z} > 0$ is a scalar. This means that all fracture compliances are equal; that is, $Z_N = Z_R = Z_T = \mathbb{Z}$. Then, because $\boldsymbol{\tau} : \mathbf{nIn} : \boldsymbol{\tau} = \boldsymbol{\tau}\cdot\boldsymbol{\tau} : \mathbf{nn}$, and equation 19 becomes

$$2\Delta f = \boldsymbol{\tau}\cdot\boldsymbol{\tau}:\frac{1}{V}\sum_k (\mathbb{Z}\mathbf{nn}A)^{(k)}, \tag{21}$$

thus, identifying the quantity $(1/V)\Sigma_k(\mathbb{Z}\mathbf{nn}A)^{(k)}$ as the proper crack-density tensor. It is symmetric and has the second rank; therefore, a material with any orientation distribution of scalar cracks is orthorhombic. Moreover, such orthorhombic media are rather special: Their anisotropy is elliptical and characterized by only four independent constants. We emphasize that

- The effective orthotropy is rooted in the (assumed) equalities $Z_N = Z_R = Z_T$.
- The crack-density tensor is derived from the elastic potential Δf.

The proportionality $\mathbf{Z} = \mathbb{Z}\mathbf{I}$ takes place for circular cracks with an accuracy dependent on the background Poisson's ratio ν_b. Implications of such a proportionality, identified by Kachanov (1980, 1992, 1993), are discussed in the next section. Schoenberg and Sayers (1995) called the cracks satisfying equation 20 scalar. Grechka et al. (2006) numerically demonstrated that approximate equality $\mathbf{Z} = \mathbb{Z}\mathbf{I}$ holds on average for multiple, noncircular cracks provided that their shape irregularities are random.

Dry circular cracks

For a circular dry crack that has radius a, the normal and shear compliances are not equal,

$$Z_N = \frac{16a(1-\nu_b^2)}{3\pi E_b} \quad \text{and} \quad Z_R = Z_T = \frac{Z_N}{1-\nu_b/2}; \tag{22}$$

however, they are relatively close because the (usually positive) Poisson's ratio ν_b satisfies inequality $\nu_b \le 1/2$. The difference between Z_N and Z_T leads to the following form of the potential Δf (Kachanov, 1980):

$$\Delta f = \frac{16(1-\nu_b^2)}{3E_b(2-\nu_b)}[(\boldsymbol{\tau}\cdot\boldsymbol{\tau}):\boldsymbol{\alpha} + \boldsymbol{\tau}:\boldsymbol{\beta}:\boldsymbol{\tau}], \tag{23}$$

where

$$\boldsymbol{\alpha} = \frac{1}{V}\sum_k (a^3\mathbf{nn})^{(k)} \tag{24}$$

and

$$\boldsymbol{\beta} = -\frac{\nu_b}{2}\frac{1}{V}\sum_k (a^3\mathbf{nnnn})^{(k)}. \tag{25}$$

Two tensors $\boldsymbol{\alpha}$ and $\boldsymbol{\beta}$ contain all information about the crack distribution over orientations and sizes relevant for the effective properties in the noninteraction approximation. The second-rank crack-density tensor $\boldsymbol{\alpha}$ can be viewed as a natural tensorial extension of the scalar crack density

$$e = \frac{1}{V}\sum_k (a^3)^{(k)} \equiv \mathrm{tr}\boldsymbol{\alpha} \tag{26}$$

defined by Bristow (1960).

Remarkably, the crack widths or the aspect ratios θ do not enter equations 23–25, implying that the effective properties of solids with dry fractures are almost independent of θ (provided that $\theta \ll 1$). Consequently, the crack-related porosity has virtually no influence on the effective elasticity.

According to equations 23 and 25, dry, circular cracks become scalar (in the terminology of Schoenberg and Sayers, 1995) only when the background has zero Poisson's ratio ν_b. In reality, $\nu_b \neq 0$; however, the influence of $\boldsymbol{\beta}$-term in equation 23 is still relatively minor as a result of the multiplier $\nu_b/2$ (equation 25) that cannot be greater than one-fourth. Hence, neglecting this term and retaining $\boldsymbol{\alpha}$ as the sole crack-density parameter constitutes a reasonable approximation; computational studies of Grechka and Kachanov (2006a; 2006b) confirm its accuracy. Thus, we are back to the conclusion drawn for the (unrealistic) scalar fractures: A solid with arbitrarily oriented circular cracks is nearly orthorhombic. Moreover, one's ability to describe the effective elasticity in terms of just $\boldsymbol{\alpha}$ results in the following important properties of the crack-induced anisotropy:

- The overall influence of multiple, differently oriented dry fracture sets is indistinguishable from that of three orthogonal sets.
- The normals to these equivalent sets coincide with the principal directions of tensor $\boldsymbol{\alpha}$; the corresponding principal crack densities are the eigenvalues of $\boldsymbol{\alpha}$.
- The crack-induced orthotropy is elliptical. Furthermore, it is controlled by only four independent quantities [the combinations of E_b, ν_b, and three eigenvalues of $\boldsymbol{\alpha}$; see Kachanov (1980; 1993) for detail] rather than nine needed for general orthotropy. This feature was exploited by Grechka and Kachanov (2006a), who proposed a fracture-characterization technique capable of handling multiple sets of vertical cracks.

Differentiating Δf given by equation 23 with respect to $\boldsymbol{\tau}$ and using definitions 9, 16, and 17, we get an equivalent result in compliances (Kachanov, 1980; Sayers and Kachanov, 1995; Schoenberg and Sayers, 1995):

$$\Delta s_{ijlm} = \frac{8(1-\nu_b^2)}{3E_b(2-\nu_b)}(\alpha_{il}\delta_{jm} + \alpha_{im}\delta_{jl} + \alpha_{jl}\delta_{im} + \alpha_{jm}\delta_{il} + 4\beta_{ijlm}), \quad (i,j,l,m = 1,2,3), \tag{27}$$

where δ_{jm} is the Kronecker delta. Either ignoring tensor $\boldsymbol{\beta}$ in equation 27 or approximating its components β_{ijlm} with $-\nu_b(\alpha_{il}\delta_{jm} + \alpha_{im}\delta_{jl} + \alpha_{jl}\delta_{im} + \alpha_{jm}\delta_{il})/8$, we recover the effective elliptical orthotropy.

In summary, the theoretically predicted effective orthotropy of a simplified type for multiple sets of dry, penny-shaped fractures is subject to two assumptions:

1) The average over cracks equality of the normal and shear fracture compliances
2) The noninteraction approximation

We will test both assumptions numerically and show that their accuracy and range of applicability are sufficient for seismic needs.

Liquid-filled fractures

The influence of liquid infill on the overall compliance was first examined by O'Connell and Budiansky (1974) and Budiansky and O'Connell (1976) for cracks with (somewhat unrealistic for rocks)

identical aspect ratios. Shafiro and Kachanov (1997) extended the analysis to fractures that have diverse aspect ratios. They generalized equation 27 to

$$\Delta s_{ijlm} = \frac{8(1-\nu_b^2)}{3E_b(2-\nu_b)}(\alpha_{il}\delta_{jm} + \alpha_{im}\delta_{jl} + \alpha_{jl}\delta_{im} + \alpha_{jm}\delta_{il} + 4\beta'_{ijlm}), \quad (i,j,l,m = 1,2,3), \tag{28}$$

where

$$\boldsymbol{\beta}' = \boldsymbol{\beta} - \frac{1}{V}\left(1 - \frac{\nu_b}{2}\right)\sum_k (\varsigma a^3 \mathbf{nnnn})^{(k)}. \tag{29}$$

The dimensionless parameters

$$\boldsymbol{\varsigma}^{(k)} = \frac{1}{1 + \theta^{(k)}[E_b/K_f - 3(1-2\nu_b)]} \tag{30}$$

are called the fluid factors. Their magnitudes are governed by the bulk modulus of fluid K_f and the crack aspect ratios $\theta^{(k)}$.

The structure of equations 29 and 30 provides important insights into the influence of fluids on the effective elasticity. Note the minus sign in front of the second term in equation 29. It implies that the presence of fluids in fractures stiffens the overall properties compared to those for dry cracks, exactly as our intuition tells us. Next, because fluids are more compliant than the background rock, the fluid factors are bounded by $0 \le \boldsymbol{\varsigma}^{(k)} \le 1$. Near zero $\boldsymbol{\varsigma}^{(k)}$ mean dry fractures ($K_f/E_b \approx 0$), while $\varsigma^{(k)} \approx 1$ indicate either thin cracks ($\theta^{(k)} \approx 0$) or a relatively stiff fluid infill or both. Increasing the aspect ratios of cracks with such a stiff infill reduces the corresponding fluid factors and makes the liquid-filled cracks look similar to dry ones, thus pointing to the importance of the aspect ratios for the effective elasticity. As a direct consequence, the crack-density tensor $\boldsymbol{\alpha}$ alone is no longer sufficient for describing the effective properties; the additional (and essential) microstructural parameters are captured by the fourth-rank tensor $\boldsymbol{\beta}'$ (equation 29).

Analysis of the magnitude of tensor $\boldsymbol{\beta}'$ reveals another apparent complication brought by the presence of fluids in cracks. Equations 24 and 29 indicate that the norms of tensors $\boldsymbol{\alpha}$ and $\boldsymbol{\beta}'$ are comparable when the fluid factors are not small. Therefore, tensor $\boldsymbol{\beta}'$ cannot be ignored similarly to tensor $\boldsymbol{\beta}$, and, in principle, the effective symmetry might be lower than orthorhombic. Nevertheless the deviations from orthotropy are expected to be small because of the stiffening effect of fluids: tensor $\boldsymbol{\beta}'$, acting in some sense opposite to $\boldsymbol{\alpha}$, weakens the overall influence of fractures. The net result is that the magnitude of crack-induced anisotropy decreases, and orthotropy still holds because of the proximity of the effective media to isotropy (Grechka and Kachanov, 2006a).

Porelike cracks

For completeness, we mention an extension of the noninteraction approximation to ellipsoidal porelike fractures whose aspect ratios are not small. The crack contribution $\Delta \boldsymbol{s}$ to the effective stiffness is given in terms of Eshelby (1957) tensor $\mathbb{S}$ as (Shafiro and Kachanov, 1997; Kachanov et al., 2003)

$$\Delta \mathbf{s} = \phi[(\mathbf{s}_i - \mathbf{s}_b)^{-1} + \mathbf{c}_b{:}(\mathbf{J} - \mathbb{S})]^{-1}, \tag{31}$$

where $\mathbf{s}_i$ is the compliance of infill material ϕ is the crack porosity (fraction of volume V occupied by the crack), and J is the fourth-rank identity tensor. We use expression 31 below to illustrate the influence of nonzero crack aspect ratios θ on the effective properties.

Schoenberg's linear slip theory

The noninteraction approximation for dry fractures and the linear slip theory (Schoenberg, 1980) have identical forms. The difference, however, is that the former yields the effective elastic constants in terms of geometric crack-density parameters (at least, for circular, elliptic, and annular fracture shapes), whereas the latter lacks a link to the microstructure (Schoenberg, 1980; Schoenberg and Sayers, 1995).

For liquid-filled fractures, Schoenberg's $\Delta \mathbf{s}$ differs from that given by equation 28 because the linear slip results were obtained by inverting Hudson's (1981) effective stiffnesses (Schoenberg and Douma, 1988). Without reproducing these equations here (they are given in Schoenberg and Douma, 1988), we note that the quantitative difference between $\Delta \mathbf{s}$ of the linear slip theory and that of equation 28 is small because of the overall weak influence of liquid-filled fractures on the effective properties.

Hudson's theory

In contrast to the noninteraction approximation that yields compliances as linear functions of the crack density e, Hudson (1980) focuses on the effective stiffnesses $\mathbf{c}_e$ and constructs them as a power series with respect to e. As we discussed in the beginning, he truncates the series after either the linear (the first-order theory) or the quadratic term (the second-order approximation).

Hudson's first-order theory (1980, 1981) has the form

$$\mathbf{c}_e = \mathbf{c}_b + \Delta \mathbf{c}. \tag{32}$$

It represents the dilute limit, which is essentially the noninteraction approximation for compliances being inverted and linearized with respect to the crack density. As demonstrated in Figure 1, such a linearization significantly reduces the accuracy of the noninteraction approximation.

For a single set of penny-shaped fractures that has the crack density e and the normal $\mathbf{n} = \mathbf{x}_1$, $\Delta \mathbf{c}$ in equation 32 is given by

$$\Delta \mathbf{c} = -\frac{e}{\mu_b} \times \begin{pmatrix} (\lambda_b+2\mu_b)^2\mathcal{U}_{33} & \lambda_b(\lambda_b+2\mu_b)\mathcal{U}_{33} & \lambda_b(\lambda_b+2\mu_b)\mathcal{U}_{33} & 0 & 0 & 0 \\ \lambda_b(\lambda_b+2\mu_b)\mathcal{U}_{33} & \lambda_b^2\mathcal{U}_{33} & \lambda_b^2\mathcal{U}_{33} & 0 & 0 & 0 \\ \lambda_b(\lambda_b+2\mu_b)\mathcal{U}_{33} & \lambda_b^2\mathcal{U}_{33} & \lambda_b^2\mathcal{U}_{33} & 0 & 0 & 0 \\ 0 & 0 & 0 & 0 & 0 & 0 \\ 0 & 0 & 0 & 0 & \mu_b^2\mathcal{U}_{11} & 0 \\ 0 & 0 & 0 & 0 & 0 & \mu_b^2\mathcal{U}_{11} \end{pmatrix}, \tag{33}$$

where λ_b and μ_b are the Lamé coefficients of the host rock. The quantities $\mathcal{U}_{11}$ and $\mathcal{U}_{33}$ are (Hudson, 1980; 1981; Peacock and Hudson, 1990)

$$\mathcal{U}_{11} = \frac{16}{3(3-2g_b)(1+\mathcal{M})}, \quad \mathcal{U}_{33} = \frac{4}{3(1-g_b)(1+\mathcal{K})}, \tag{34}$$

$$\mathcal{M} = \frac{4\mu_i}{\pi\theta(3-2g_b)\mu_b}, \quad \mathcal{K} = \frac{\lambda_i + 2\mu_i}{\pi\theta(1-g_b)\mu_b}, \tag{35}$$

$$g_b = \frac{V_{S,b}^2}{V_{P,b}^2} = \frac{\mu_b}{\lambda_b + 2\mu_b} = \frac{1 - 2\nu_b}{2(1 - \nu_b)}, \tag{36}$$

where $V_{P,b}$ and $V_{S,b}$ are the P- and S-wave velocities of the background, λ_i and μ_i are the Lamé parameters of the infill, and all cracks are assumed to have the same aspect ratio θ. If L differently oriented fracture sets are present, their stiffness contributions $\Delta\mathbf{c}^{(\ell)}$ are simply summed up (Hudson, 1981),

$$\Delta\mathbf{c} \to \sum_{\ell=1}^{L} \Delta\mathbf{c}^{(\ell)}. \tag{37}$$

Substitution 37 is insensitive to the spatial distribution of fractures as it should be in the noninteraction approximation.

Hudson's second-order theory (1980; 1991) extends linear approximation 32 by adding the term quadratic in the crack density:

$$\mathbf{c}_e = \mathbf{c}_b + \Delta\mathbf{c} + \Delta\Delta\mathbf{c}, \tag{38}$$

where

$$\Delta\Delta\mathbf{c} = \frac{1}{\mu_b}\Delta\mathbf{c}:\boldsymbol{\chi}:\Delta\mathbf{c}, \tag{39}$$

$$\chi_{ijkl} = \frac{1}{15}[\delta_{ik}\delta_{jl}(4 + g_b) - (\delta_{il}\delta_{jk} + \delta_{ij}\delta_{kl})(1 - g_b)],$$

$$(i,j,k,l = 1,2,3), \tag{40}$$

and g_b is given by equation 36. Note that the second-order term (equation 39) is constructed from the first-order one (equation 33) without bringing in any additional information about the fractures. We refrain from discussing the validity of Hudson's theory here and, instead, let equations 32 and 38 speak for themselves in the examples below.

NUMERICAL VALIDATION

We now compare predictions of different theories to 3D finite-element simulations of the effective elasticity. We examine a number of fracture geometries clearly violating our key theoretical assumptions (the absence of crack interactions, equality $Z_N = Z_T$, circular crack shapes) and yet discover that the noninteraction approximation (equations 23 or 27) is robust and satisfactorily accurate in the entire range of crack densities expected in naturally fractured reservoirs.

Single set of dry, penny-shaped cracks

We start with the simplest fracture geometry — a single set of vertical, isolated, penny-shaped cracks — that has been extensively studied in the past (e.g., Hudson, 1980; 1981; Schoenberg, 1980; 1983; Schoenberg and Douma, 1988; Hsu and Schoenberg, 1993; Thomsen, 1995; Hudson et al., 1996; Bakulin et al., 2000). The effective media for such crack arrays are known to be transversely isotropic with a horizontal symmetry axis (HTI) pointing in the direction normal ($\mathbf{n} = \mathbf{x}_1$) to the fracture faces. Here we will to do the following:

- Compare Schoenberg's and Hudson's predictions of the effective stiffness $\mathbf{c}_e$.
- Evaluate the importance of fracture interactions via finite-element modeling.
- Examine the influence of nonzero aspect ratios on $\mathbf{c}_e$.

Schoenberg's versus Hudson's predictions

Figure 1 compares several predictions of the effective stiffness coefficients $c_{e,11}$ and $c_{e,22}$ for a single set of dry circular cracks. The results of Schoenberg (★) and the noninteraction approximation (◯) almost coincide and are close to those of finite-element modeling (bars; we discuss the numerical simulations in more detail below). Hudson's predictions (marked with ▽ and △) significantly deviate from them.

Grechka and Kachanov (2006a) investigated the issue of negative $c_{e,11}$ predicted by the first-order theory of Hudson (▽ in Figure 1) and found [based on equation 21 of Hudson (1981) or on equations 20a and 24b of Liu et al. (2000)] that

$$c_{e,11}(e) < 0 \quad \text{when} \quad e > \frac{3}{4}g_b(1 - g_b), \tag{41}$$

where g_b is given by equation 36. Similar analysis utilizing matrix 33 yields for $c_{e,22}$

$$c_{e,22}(e) < 0 \quad \text{when} \quad e > \frac{3g_b(1 - g_b)}{4(1 - 2g_b)^2}. \tag{42}$$

Both these inequalities indicate that Hudson's first-order scheme encounters problems for small $V_{S,b}/V_{P,b}$ ratios or, equivalently, for large Poisson's ratios ν_b (equation 36). Interestingly, the first-order Hudson's theory breaks down for any nonzero crack density of dry fractures in the limit $g_b \to 0$. Its accuracy improves for greater g_b but still remains inferior to that of the linear slip theory. Also, Hudson's pre-

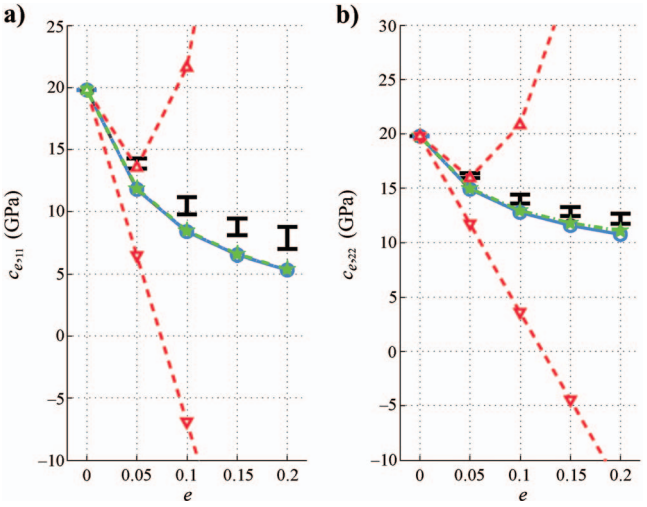

Figure 1. Effective stiffness coefficients (a) $c_{e,11}$ and (b) $c_{e,22}$ for a single set of dry cracks. The background velocities are $V_{P,b} = 3.0$ km/s; $V_{S,b} = 1.0$ km/s; and density is $\rho_b = 2.2$ g/cm^3. They yield Lamé coefficients $\lambda_b = 15.4$ GPa, $\mu_b = 2.2$ GPa. Symbols indicate different theoretical predictions: red ▽ — the first-order Hudson's (equations 32 and 33), red △ — the second-order Hudson's (equations 33 and 38–40), green ★ — Schoenberg's (equations 9 and 24–27), and blue ◯ — the noninteraction approximation (equations 9 and 31) that takes into account nonzero crack aspect ratios ($\theta = 0.05$ for all fractures). Bars correspond to the 95% confidence intervals (the mean values ±2 standard deviations) of the numerically computed stiffness coefficients obtained for 100 random realizations of the fracture locations.

dictions are not as poor for shear moduli $c_{e,44}$, $c_{e,55}$, and $c_{e,66}$ (not shown).

The second-order theory of Hudson (equations 38–40 and 33, marked with △ in Figure 1) results in obviously incorrect, monotonically growing $c_{e,11}(e)$ and $c_{e,22}(e)$ at $e \gtrsim 0.05$. Such a behavior implies that adding fractures *stiffens* rather than softens the rock. This theory leads to another, equally unphysical prediction: $c_{e,11}(e)$ and $c_{e,22}(e)$ exceed their background values $c_{e,11}(0) = c_{e,22}(0) = \lambda_b + 2\mu_b = 19.8$ GPa at $e \gtrsim 0.09$, thus indicating that a solid containing fractures is stiffer than the uncracked one. In fact, the tendency of the second-order Hudson's theory to produce unreasonably high effective stiffnesses displayed in Figure 1 has been known for quite some time both for a single fracture set and for randomly oriented cracks (Sayers and Kachanov, 1991; Cheng, 1993). Jakobsen et al. (2003) recently showed that the same tendency holds for an arbitrary distribution of fractures. Grechka and Kachanov (2006a) numerically confirmed findings of Jakobsen et al. (2003) for multiple sets of cracks.

Additional insights into the behavior of effective elastic properties can be gained by examining the anisotropic coefficients $\epsilon^{(V)}$, $\delta^{(V)}$, and $\gamma^{(V)}$ (Figure 2) introduced for HTI media by Rüger (1997) and Tsvankin (1997). Figure 2a and b does not display the first-order Hudson's predictions for $\epsilon^{(V)}$ and $\delta^{(V)}$ because they fall out of the scale ranges there. Let us make the following observations:

- The linear slip theory (green ★) indicates that $\epsilon^{(V)} \approx \delta^{(V)}$; therefore, an approximate elliptical anisotropy ($\eta^{(V)} \approx \epsilon^{(V)} - \delta^{(V)} \approx 0$) is expected.
- It has been pointed out in many papers (see Bakulin et al., 2000, for a review) that the shear-wave splitting coefficient is close to the crack density, $|\gamma^{(V)}| \approx e$. Figure 2c clarifies that this conclusion is based mainly on Hudson's theory (red ▽ and △). While equality $|\gamma^{(V)}| \approx e$ is not supported by the linear slip theory at large-crack densities, it might be viewed as a reasonable (but unnecessary) approximation at smaller crack densities, say, when $e \lesssim 0.1$.

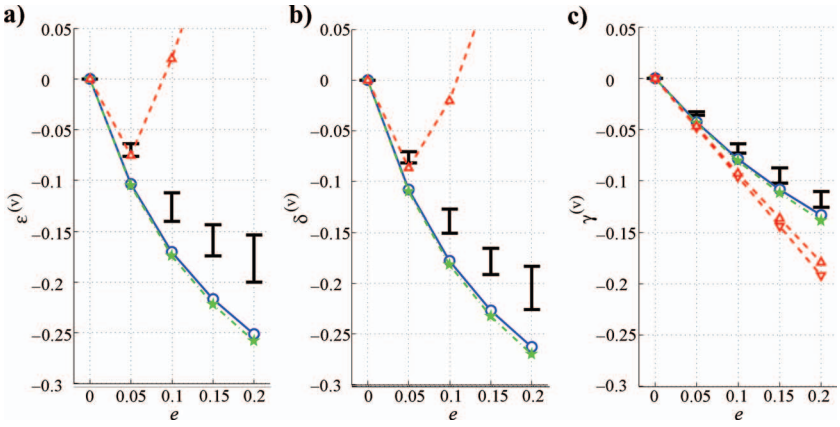

Figure 2. Effective anisotropic coefficients (a) $\epsilon^{(V)}$, (b) $\delta^{(V)}$, and (c) $\gamma^{(V)}$. The symbols are the same as those in Figure 1.

Overall, we conclude that the linear slip theory (or the noninteraction approximation in compliances) is superior to either first- or second-order Hudson's schemes for a single set of dry penny-shaped cracks.

Fracture interactions

We now discuss the finite-element modeling (done with software COMSOL, 2005) that led to bars shown in Figures 1 and 2. The computations were performed following the methodology described by Grechka (2003; 2005). We simulate the remote stress boundary conditions by applying constant loads to faces of a homogeneous cube that has the background properties ($\mathbf{c}_b$) and envelops the fractured volume V (this approach is called the framing method in computational mechanics).

Let us explain the origin of the bars or the scatter in effective parameters at a given crack density e. The reason for the scatter is the interaction in the stress fields of the adjacent cracks. Figure 3 shows the local behavior of the stress component τ_{11}. When the locations of crack centers (that are supposed to be random) vary in V, the patterns of interactions change, introducing variations in the numerically computed effective stiffness tensors $\mathbf{c}_e$. Such variations, which are inevitable for any finite-number of cracks (e.g., Zohdi and Wriggers, 2001), are indicative of deviations of our volumes V from the true, albeit unattainable in practice, representative volume. Bearing this issue in mind and relying on the results already established in computational micromechanics (Zohdi and Wriggers, 2005), we have chosen 15 isolated fractures for our tests. The bars in Figures 1 and 2 correspond to the 95% confidence intervals in the computed quantities estimated from 25 random realizations of the crack locations for each crack density $e = 0.05, 0.10, 0.15$, and 0.20.

Note that bars in Figures 1 and 2 are located above the predictions of the noninteraction approximation (★ and ◯). To understand why it is so, we need to examine Figure 3 more closely. We observe two types of the stress disturbances caused by cracks: relatively extended areas of low stress called the shielding (blue) and smaller areas of elevated stress called the amplification (yellow and red). The physical reason for shielding is easy to grasp. The crack faces are traction free because the cracks are dry. This means that $\tau_{11} = 0$ at the faces of all fractures regardless of the applied remote load. As the stress is con-

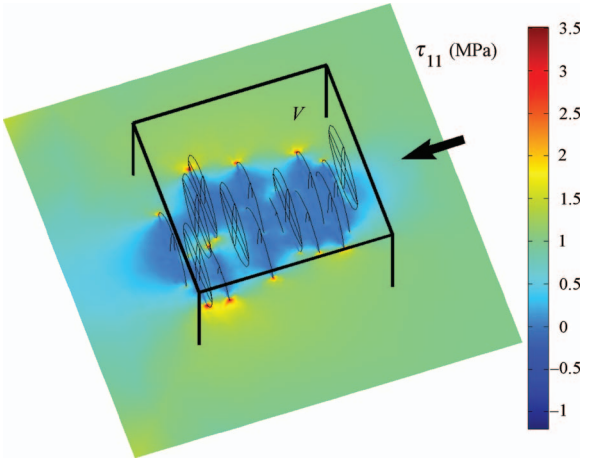

Figure 3. Horizontal cross section of stress component τ_{11} through a typical model that contains 15 dry fractures (wire spheroids). The crack density is $e = 0.15$. Arrow shows the direction of applied remote load; its magnitude is 1 MPa. Cubes in this and other similar figures indicates the boundaries of volume V that contains cracks. (See text above for the explanation of the colors.)

tinuous in the background, it slowly gets back from zero to its far-field value as the distance from a crack face increases. On the other hand, the stress obeys an analog of the Gauss divergence theorem for linear elasticity (e.g., Markov, 1999). The theorem says that the volume integrals of the stress components are equal to the surface integrals of the applied constant loads. Therefore, there have to be areas of higher τ_{11} that would compensate for the presence of the low τ_{11} in the vicinity of fracture faces and yield the proper volume average. These stress-amplification areas always form at the fracture tips. Figure 3 demonstrates that the shielding occupies a major portion of volume V, and hence, dominates the amplification. As a result, the numerically computed effective media come out to be stiffer than those predicted by the noninteraction approximation. Figure 1 illustrates it directly. The stiffening naturally translates into a reduction of the magnitude of the crack induced anisotropy; this is why bars in Figure 2 correspond to smaller absolute values of the anisotropic coefficients than those shown with the green ★ and the blue ◯.

Note that Saenger et al. (2004) observe quite an opposite, softening effect of the crack interactions in their finite-difference wave-propagation experiments. At this point, it is unclear what causes such a discrepancy in the numerical results obtained with different methods. We suggest that further numerical studies are needed to clarify this issue.

We can now assess the accuracy of the noninteraction approximation. If we take a view that errors in the interval anisotropic coefficients estimated from seismic data are seldom smaller than 0.05 (high-accuracy cross-dipole sonic logs and vertical seismic profile data might be the exceptions), the predictions of the linear slip theory are satisfactory up to the crack density of about 0.15 for $\epsilon^{(V)}$ and $\delta^{(V)}$ and in the whole range $0 \le e \le 0.2$ for $\gamma^{(V)}$. Either of these values covers the range of crack densities expected in naturally fractured reservoirs. Interestingly, Grechka and Kachanov (2006a; b) show that the noninteraction approximation tends to perform even better for multiple fracture sets because diversity in the crack orientations leads to a more complete cancelation of the competing effects of the stress shielding and amplification.

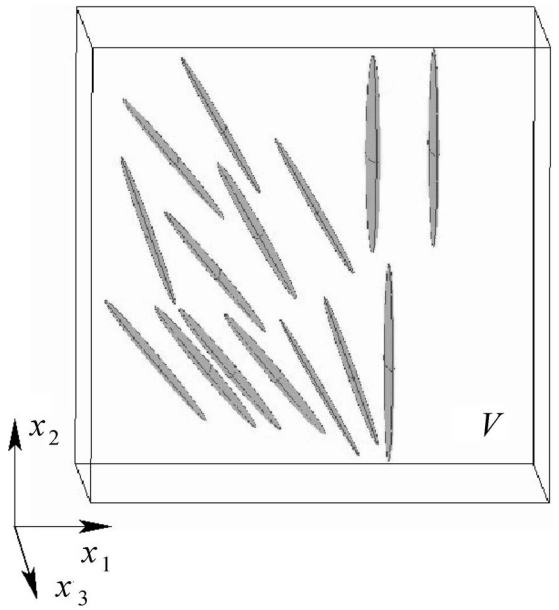

Figure 4. Nearly plan view of a typical model containing four vertical fracture sets. The presence of two orthogonal vertical planes of elastic symmetry is not obvious from the crack geometry.

Influence of nonzero aspect ratios

In addition to displaying the crack-interaction patterns, Figure 3 also illustrates the insensitivity of the effective properties to the crack aspect ratios. Indeed, all crack faces reside in the areas of near-zero stresses. Therefore, widening or thinning a crack would either remove or add the host-rock volumes that contribute to the overall averages quite weakly because the stresses (and strains) are small there. Figure 2, which shows the influence of a variation of the aspect ratios from $\theta = 0$ (★) to $\theta = 0.05$ (◯) on the effective anisotropic coefficients, directly confirms the virtual absence of such an influence.

Figure 3 allows us to make a more general inference about the influence of shapes of fracture faces on the effective stiffness $\mathbf{c}_e$. Suppose that smooth faces of our penny-shaped cracks become slightly rough (such cracks are called microcorrugated). If their jaggedness is limited to the areas of vanishingly small background stresses and strains, it has almost no influence on the effective elasticity. Below, we give an example of such a microcorrugated fracture and show that its stiffness contribution $\Delta\mathbf{c}$ is equivalent to that of an elliptic crack with smooth faces.

Multiple sets of penny-shaped cracks

Next, we examine the effective anisotropy caused by several sets of nonparallel vertical cracks. We establish an approximate overall orthorhombic elastic symmetry for nonintersecting circular fracture arrays despite the fact that the crack geometries do not possess it. The same conclusion is then extended to more realistic intersecting cracks than might create interconnected fracture networks.

Effective orthotropy

Let us turn our attention to multiple sets of nonintersecting penny-shaped fractures. The noninteraction scheme predicts that the crack-induced effective stiffness tensors $\mathbf{c}_e$ are almost orthorhombic regardless of the number of fracture sets and their orientations. Deviations of $\mathbf{c}_e$ from orthotropy potentially can be caused by the following factors:

- The fourth-rank tensor $\boldsymbol{\beta}$ (equation 25) for dry fractures when $\nu_b \neq 0$
- The fourth-rank tensor $\boldsymbol{\beta}'$ (equation 29) for liquid-filled fractures
- Nonzero crack aspect ratios
- Fracture interactions

Here we examine the cumulative influence of all these factors by performing finite-element calculations of $\mathbf{c}_e$ for crack arrays that contain four vertical fracture sets oriented at azimuths $\varphi_1 = 0°$, $\varphi_2 = 20°$, $\varphi_3 = 30°$, $\varphi_4 = 40°$ with respect to the coordinate axis $\mathbf{x}_1$. The crack density associated with the first set varies from $e_1 = 0$ to $e_1 = 0.09$ while the crack densities of other three sets are kept fixed at $e_2 = 0.01, e_3 = 0.02$, and $e_4 = 0.03$. This makes the total crack density $e = \Sigma_{\ell=1}^{4} e_\ell$ (defined by equation 26) change from $e = 0.06$ to $e = 0.15$.

We generate 25 crack arrays (such as that shown in Figure 4) for each of the total crack densities $e = [0.06, 0.09, 0.12, 0.15]$ by randomly varying the number of cracks (from 10 to 100), their aspect ra-

tios (from 0.04 to 0.08), and the locations of their centers. For each fracture array, we compute the effective stiffness tensor $\mathbf{c}_e$ and calculate its percentage deviations Δ_e^{ort} from orthotropy

$$\Delta_e^{\text{ort}} = \frac{\max|\mathbf{c}_e - \mathbf{c}_e^{\text{ort}}|}{\max|\mathbf{c}_e|} \times 100\%, \tag{43}$$

where the components of $\mathbf{c}_e^{\text{ort}}$ are obtained from $\mathbf{c}_e$ by letting

$$c_{e,ijlm}^{\text{ort}} = \begin{cases} 0 \text{ when } \quad \delta_{ij}\delta_{lm} + \delta_{il}\delta_{jm} + \delta_{im}\delta_{jl} = 0 \text{ and} \\ c_{e,ijlm} \text{ otherwise,} \quad (i,j,l,m = 1,2,3). \end{cases} \tag{44}$$

Figure 5 displays the 95% confidence intervals for Δ_e^{ort} for our 100 crack arrays. Clearly, all effective stiffness tensors $\mathbf{c}_e$ are virtually orthorhombic. This means that the factors listed above are weak and therefore unimportant.

Figure 5 also shows that Δ_e^{ort} are smaller for water-filled cracks than for dry ones even though $\|\boldsymbol{\beta}'\|$ (equation 29) is significantly greater than $\|\boldsymbol{\beta}\|$ (equation 25). The reason for that is the stiffening effect of fluids. For example, the largest effective anisotropic coefficient $|\delta^{(1)}| = 0.20$ for dry cracks and only $|\delta^{(1)}| = 0.06$ when the fractures are filled with water (all effective media in this test are monoclinic; their anisotropic coefficients were introduced by Grechka et al., 2000). Thus, we conclude that the crack-induced anisotropy is orthorhombic (with a good accuracy) for any type of fluid infill. While this property is generic and follows from equality $Z_N \approx Z_T$ (second equation 22) for dry cracks, it stems from the proximity of effective media to isotropy when the fractures are filled with a liquid.

Another, rather trivial, consequence of a relatively weak magnitude of anisotropy for liquid-filled cracks is that all effective media schemes, including those of Hudson (1980), become sufficiently accurate for seismics. Although their predictions are still different, they all are close to each other and to the numerically generated stiffness tensors (Grechka and Kachanov, 2006a). The reason is simple: Relatively small fracture contributions do not give room for large errors in the effective properties. The presence of pores in the background rock makes it more compliant and thus further reduces the influence of fractures on the effective elasticity. It gives rise, however, to a host of other issues related to the pressure equilibration and fluid flow between the pores and fractures. They are outside the scope of our tutorial. (See Cardona, 2002 and Gurevich, 2003 for a current discussion.)

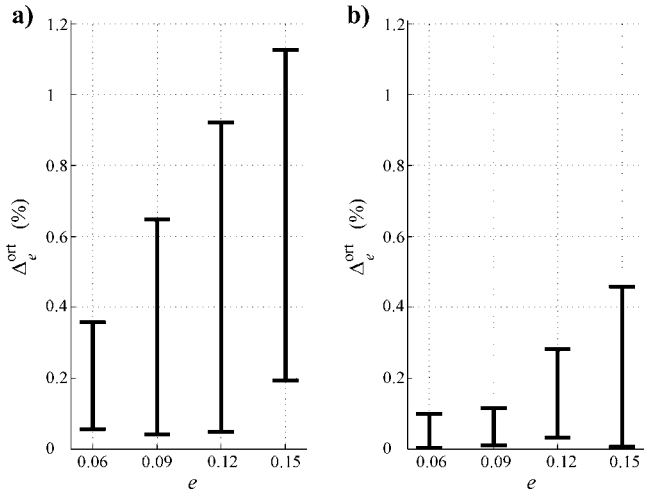

Figure 5. Relative deviations of the effective stiffness tensors from orthotropy for (a) dry and (b) water-filled fractures. Bars are the 95% confidence intervals of Δ_e^{ort} (equations 43 and 44). The background Poisson's ratio is $\nu_b = 0.45$.

Intersecting cracks

We now make another step toward reality and allow the fractures to intersect each other and possibly form interconnected networks. Because no theory exists to predict the effective elasticity of solids with intersecting cracks, we have to resort to numerical modeling. Even though fracture intersections violate the main assumption of the noninteraction approximation, we still compare its predictions with our finite-element results to find out whether the former provides a reasonable proxy for the numerically obtained effective stiffnesses $\mathbf{c}_e$.

Here, following Grechka and Kachanov (2006b), we examine 175 arrays that contain both the nonintersecting and intersecting cracks. We compute their effective anisotropic coefficients with the finite-element method and compare their values with those predicted by the noninteraction approximation. The models in this test have three sets of vertical, dry, circular cracks oriented at azimuths $\varphi_1 = 0°$, $\varphi_2 = 30°$, and $\varphi_3 = 40°$ with respect to the coordinate axis $\mathbf{x}_1$. The crack densities of sets 2 and 3 are fixed at $e_2 = 0.02$ and $e_3 = 0.06$, while the density of set 1 changes from $e_1 = 0$ to $e_1 = 0.06$ making the total crack density $e = \Sigma_{\ell=1}^{3} e_\ell$ vary from 0.08 to 0.14. Figure 6 displays our typical fracture arrays. Note that intersecting fractures create intricate geometries ranging from relatively simple X-, 8-, and V-shapes (Figure 6b and c) to more complicated ones shown in Figure 6d. Clearly, once we begin dealing with these geometries, our cracks are no longer penny shaped; they even cease to be planar.

Are fracture intersections important for the effective properties? Figure 7 gives the answer. We observe that literally nothing happens to the stress fields in the vicinities of crack intersections. Therefore, the latter have little influence on the effective elasticity and can be safely ignored. Figure 8 substantiates the statements above. It shows anisotropic coefficients of the effective (monoclinic) media for mod-

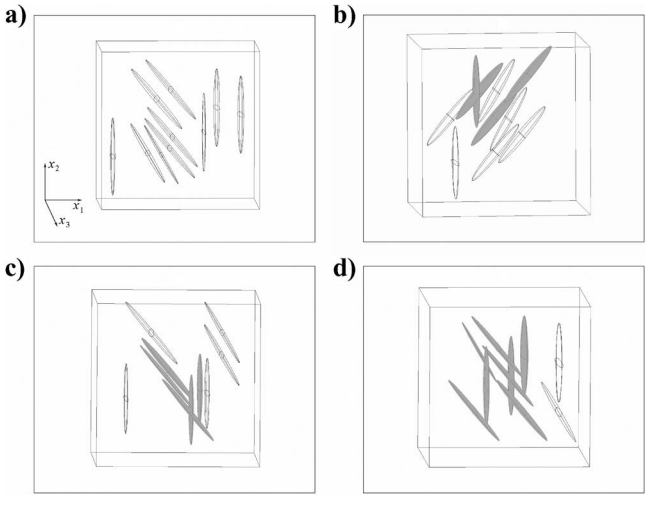

Figure 6. Arrays of (a) nonintersecting and (b, c, d) intersecting fractures. The cracks that geometrically intersect their neighbors are shaded. The aspect ratios θ of fractures lie in the range $0.04 \le \theta \le 0.08$.

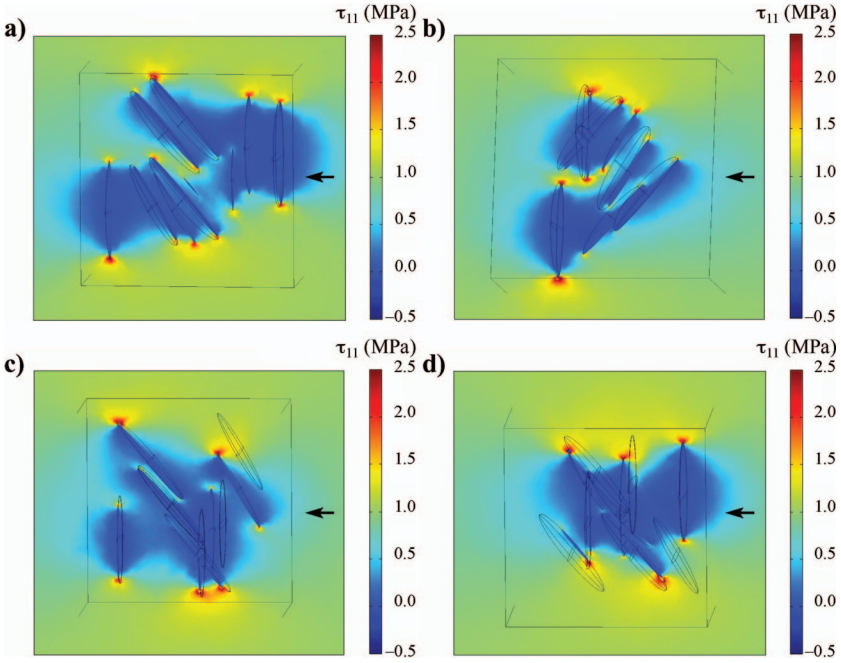

Figure 7. Horizontal cross sections of the stress component τ_{11} for crack arrays shown in Figure 6. Arrows indicate the directions of applied uniaxial remote load whose magnitude is 1 MPa.

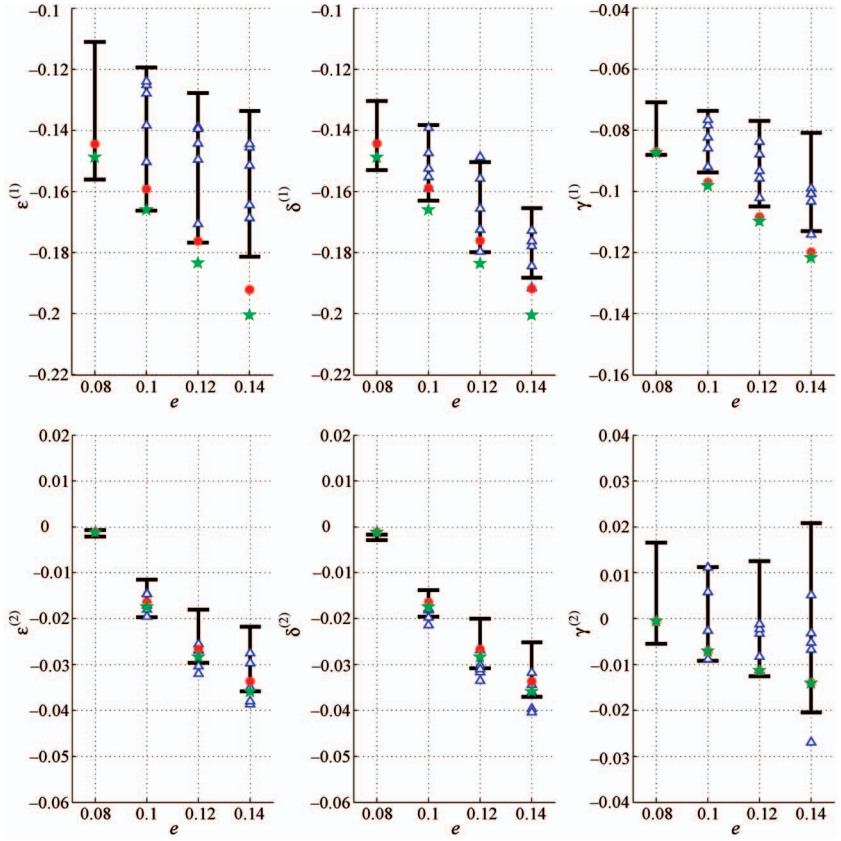

Figure 8. Effective anisotropic coefficients of fractured media. Bars correspond to the 95% confidence intervals (the mean ±2 standard deviations) of the numerically computed anisotropic coefficients. Triangles indicate their values for models with intersecting cracks. Predictions of the linear slip theory that ignores the nonzero crack aspect ratios (equations 9 and 24–27) and the noninteraction approximation that accounts for them (equations 9 and 31) are shown with and a green ★ and a red ●, respectively.

els containing nonintersecting and intersecting fractures. Bars in Figure 8 correspond to the 95% confidence intervals for the anisotropic coefficients obtained from our finite-element simulations for 40 random realizations of locations of the nonintersecting fractures at each total crack density $e = [0.08, 0.10, 0.12, 0.14]$. Triangles indicate the same coefficients, except for models where the fractures intersect each other (such as those in Figure 6b–d). Let us observe the following:

- Bars and triangles overlap implying the absence of influence of crack intersections on the effective anisotropy.
- Both the linear slip and noninteraction predictions (stars and circles) tend to slightly overestimate the magnitudes of anisotropic coefficients. Similarly to models with a single fracture set (Figure 3), it is a consequence of stiffening resulting from fracture interactions.
- Stars (equations 9 and 24–27) and circles (equations 9 and 31) in Figure 8 do not significantly deviate from each other, confirming insensitivity of the effective properties to the aspect ratios of dry cracks.

Thus, the main message of this section is that geometrical intersections of fractures make virtually no impact on the effective elasticity. The same conclusion was drawn by Saenger et al. (2004), who performed the finite-difference wave-propagation experiments rather than static modeling.

Noncircular fractures

Natural fractures in rocks are notoriously irregular. Because their shapes resemble neither circles nor ellipses, it is unclear to what extent the existing theoretical results are applicable to such geometries. Numerical simulations are obviously necessary to answer this question. Here, following Grechka et al. (2006), we illustrate the following statement: circular, penny-shaped fractures can legitimately be used to represent flat irregular cracks when the shape irregularities are random.

We examine six irregular fracture shapes shown in Figure 9. Let us use each of the geometries in Figure 9 to build a single vertical fracture set and allow the cracks in this set to have not only random locations but also random orientations (or angles) in the $[\mathbf{x}_2, \mathbf{x}_3]$-plane. We would like to know whether these irregular fractures can be replaced with penny-shaped ones for the purpose of obtaining the effective stiffnesses. The problem at hand is nontrivial even though both effective solids are transversely isotropic with an HTI. The reason is that circular fractures form a special kind of HTI characterized by fewer than five independent parameters (Schoenberg and Douma,

1988; Kachanov, 1992; Thomsen, 1995; Tsvankin, 1997; Bakulin et al., 2000). Therefore, the real issue we are addressing here is whether the ratio Z_N/Z_T for circular cracks can approximate the ratio $Z_N/\langle Z_T\rangle$ for irregular ones, where $\langle Z_T\rangle$ is the average tangential compliance in the fracture $[\mathbf{x}_2,\mathbf{x}_3]$-plane. We restrict the analysis below to dry cracks because their influence on the effective properties is much stronger than that of liquid-filled ones.

We compute the effective stiffnesses $\mathbf{c}_e$ numerically for six fracture geometries in Figure 9, average over rotations in the $\mathbf{c}_e$ in the $[\mathbf{x}_2,\mathbf{x}_3]$-plane (this yields $\langle\mathbf{c}_e\rangle$), and calculate the crack contribution to the effective stiffness,

$$\langle\Delta\boldsymbol{c}\rangle = \langle\boldsymbol{c}_e\rangle - \boldsymbol{c}_b. \tag{45}$$

Then we use equations 9 and 31 to get

$$\Delta\boldsymbol{c}^{\rm ps}(e^{\rm fit},\theta^{\rm fit}) = \boldsymbol{s}_e^{-1} - \boldsymbol{c}_b \tag{46}$$

for penny-shaped cracks. Their crack densities $e^{\rm fit}$ and aspect ratios $\theta^{\rm fit}$ are the fitting parameters. They are obtained from a nonlinear optimization $\langle\Delta\mathbf{c}\rangle \sim \Delta\mathbf{c}^{\rm ps}(e^{\rm fit},\theta^{\rm fit})$. The fit quality is quantified by the stiffness misfits

$$\Delta_c = \langle\Delta\mathbf{c}\rangle - \Delta\mathbf{c}^{\rm ps}. \tag{47}$$

We intentionally compare the stiffness contributions $\Delta\mathbf{c}$ rather than the effective stiffness tensors themselves because the former are much more sensitive to the fractures. Figure 10 shows the magnitudes of misfits Δ_c calculated in the norm

$$\Delta_c^{\rm nrm} = \frac{\max|\Delta_c|}{\max|\langle\Delta\mathbf{c}\rangle|}\times 100\%. \tag{48}$$

The misfits $\Delta_c^{\rm nrm} < 0.65\%$ for all our fracture geometries. Clearly, irregular fracture shapes in Figure 9 can be accurately represented by circular cracks. Figure 10 extends the conclusion drawn by Kachanov (1992, 1993) for elliptic cracks with random eccentricities to irregular fracture shapes.

Let us note that geometries in Figure 9 are quite complex. They include both convex and concave shapes; moreover, the fractures 4 through 6 contain islands of cohesion between the crack faces. Still, none of the $\Delta_c^{\rm nrm}$ values stands out in Figure 10, implying that the circular-crack approximation performs well for all fracture shapes.

Thus, the presented numerical tests indicate that flat cracks with random shape irregularities and random spatial locations can be represented by circular ones as far as the effective elasticity is concerned. While we discussed only dry fractures, our conclusion also remains valid for liquid-filled cracks because a much weaker influence of the latter on the effective elasticity makes details of their fracture shapes even less important. Our ability to replace irregular cracks with circular ones also implies that the effective elliptical orthotropy should hold for the former as well as it does for the latter. Grechka et al. (2006) confirmed this statement explicitly for multiple sets of rectangular cracks (model 1 in Figure 9).

Microcorrugated fractures

Finally, we discuss the so-called microcorrugated fractures whose surfaces are nonsmooth. It has been suggested (e.g., Berg et al., 1991) that a small jaggedness of the fracture faces might cause a coupling between the normal and tangential to the crack tractions and slips and thus give rise to the nonzero off-diagonal elements of the fracture-compliance tensor $\mathbf{Z}$. Several authors (Berg et al., 1991; Bakulin et al., 2000; Grechka et al., 2003) examined the influence of microcorrugation on the effective properties by assigning nonzero values to the off-diagonal elements of $\mathbf{Z}$. Here we show that, in fact, the coupling is almost absent, and

$$Z_{ij} \approx 0 \quad (i \neq j) \tag{49}$$

for approximately planar microcorrugated fractures in isotropic host rocks. Equality 49 follows from the basic principles of mechanics of heterogeneous materials — the so-called "modification" theorem of Hill (1963). It says that contribution of an irregularly shaped crack to the effective elasticity is bounded by contributions of two cracks whose shapes inscribe and circumscribe the original one. As microcorrugation can easily be smoothed out, Hill's bounds are tight, and, consequently, a slight roughness can be ignored for the effective properties (see Sevostianov and Kachanov, 2002 and Kachanov and Sevostianov, 2005 for further discussion).

We illustrate Hill's theorem on a W-shaped fracture shown in Figure 11. While its geometric jaggedness is obvious, no corresponding

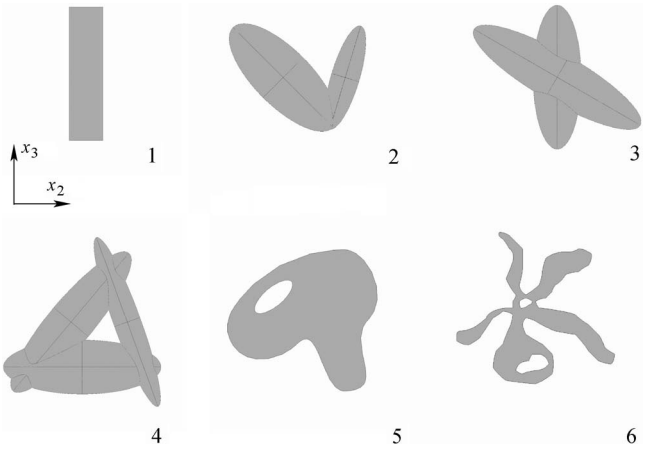

Figure 9. Irregular vertical cracks. All fractures are planar; their normals are directed along the $\boldsymbol{x}_1$-axis. The faces of cracks 2, 3, and 4 have sharp edges. Geometries 4, 5, and 6, that contain interior rock islands, represent partially closed fractures.

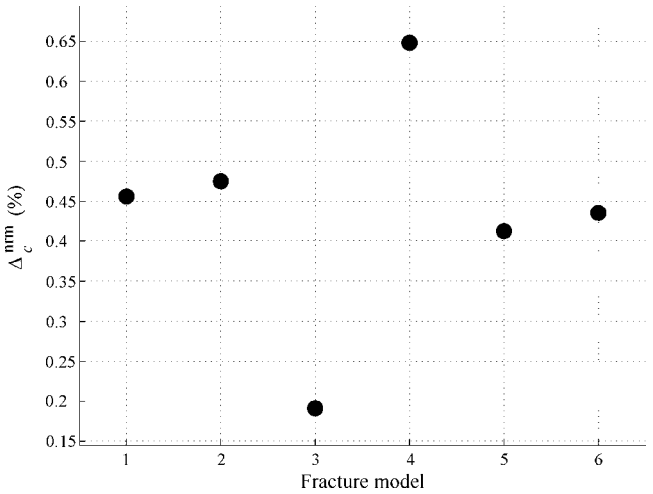

Figure 10. Misfits $\Delta_c^{\rm nrm}$ (equation 48) for six fracture shapes in Figure 9.

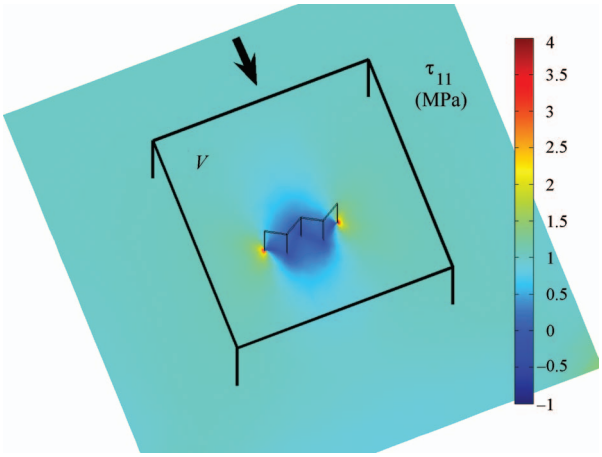

Figure 11. Horizontal cross section of the stress component τ_{11} for microcorrugated W-shaped fracture. Arrow indicates the direction of applied remote load whose magnitude is 1 MPa.

imprint in the overall pattern of stress distribution is observed. This unequivocally means that microcorrugation is unimportant and that our W-shaped crack influences the effective elasticity the same way as does an elliptic fracture with smooth faces. Direct computation confirms it. The normalized difference $\max|\Delta\mathbf{c} - \Delta\mathbf{c}^{ell}|/\max|\Delta\mathbf{c}|$ between the stiffness contribution $\Delta\mathbf{c}$ of the fracture in Figure 11 and its elliptic approximation, $\Delta\mathbf{c}^{ell}$, is only 0.15%.

In general, we can state that contributions of microcorrugated and elliptic cracks to the effective stiffness are equivalent; therefore, roughness of fracture faces does not matter for the overall elastic properties.

CONCLUSIONS

Restricting the scope to the model of fractures as highly compliant inclusions in a stiff matrix, we consistently applied the well-known noninteraction approximation derived for penny-shaped cracks to predict the effective elasticity of fracture arrays that explicitly violated the underlying assumptions of this approximation. Specifically, our cracks had irregular shapes, and their faces were nonsmooth with possible areas of partial contacts. In addition, the examined fractures strongly interacted, could intersect each other, and formed interconnected networks. Yet, the simplest noninteraction approximation was found to be satisfactory in all cases. Thus, this is the single most important message of our tutorial: *The noninteraction approximation formulated in compliances for penny-shaped fractures is relevant and sufficiently accurate for irregular and intersecting approximately flat cracks*.

There are several other points that might be relevant under specific circumstances.

Dry fractures have the strongest impact on the effective elasticity. It is particularly important to describe it using the compliance-based formulations. We show that Schoenberg's linear slip theory which is essentially the noninteraction approximation in compliances, is significantly more accurate than the theory of Hudson. Furthermore, the effective crack-induced anisotropy is nearly orthorhombic regardless of the number of fracture sets, their orientations, and the associated crack densities. We confirmed this conclusion numerically for strongly interacting and intersecting dry fractures.

Micromechanics analysis identified a number of geometric features of cracks that are insignificant for the effective properties. These features are

- Fracture intersections
- Microcorrugation of fracture faces
- Random irregularities of fracture shapes, provided that the cracks are flat

On the other hand, partial contacts of fracture faces appreciably stiffen the effective media. Still, their influence can be described adequately by circular fractures that have an appropriate crack density.

Liquid infill of fractures may significantly reduce their influence on the overall elastic properties. In this case, many effective media schemes (e.g., Schoenberg's and Hudson's) yield comparable predictions, and the choice of a particular scheme is not critical for the final result.

ACKNOWLEDGMENTS

The authors thank Shell International E & P Inc. for supporting this work. We are grateful to professors Boris Gurevich (Curtin University) and Tarek Zohdi (University of California, Berkeley) for their useful insights and suggestions.

APPENDIX A

OVERVIEW OF LITERATURE ON EFFECTIVE ELASTICITY OF CRACKED SOLIDS

Finding effective elastic properties of cracked materials is a classical problem. It has been addressed both in materials science and geophysics. We start our overview with the developments made in solid mechanics because they began some twenty years earlier than those in exploration geophysics.

Solid mechanics and materials science

Bristow (1960) was the first who gave explicit results for the effective (or overall) elasticity of fractured solids. His work rested on two assumptions: The elastic interactions between cracks were ignored (the so-called noninteraction approximation), and the crack orientations were random resulting in the overall isotropy. Importantly, he identified the scalar crack density e (equation 26) as the proper effective parameter. It represents individual cracks in accordance with their actual contributions to the overall compliances, that is, proportionally to their sizes cubed.

Kachanov (1980) extended the noninteraction approximation to general effective anisotropy due to arbitrarily oriented dry fractures embedded in an otherwise isotropic background. He obtained a somewhat counterintuitive result: the effective elasticity is nearly orthorhombic for any orientation distribution of dry cracks. Moreover, the crack-induced orthotropy turns out to be of a simplified type. It is fully described by only four independent parameters compared to nine needed for general orthotropy. Also Kachanov (1980) defined the tensorial crack-density parameters: the second-rank crack density tensor $\boldsymbol{\alpha}$ (equation 24), which generalizes the scalar crack density, and the fourth-rank tensor $\boldsymbol{\beta}$ (equation 25). The magnitude of $\boldsymbol{\beta}$ is usually much smaller than that of $\boldsymbol{\alpha}$, so the symmetry planes of effective orthorhombic media are approximately co-ori-

ented with the principal directions of $\boldsymbol{\alpha}$. A special case of two or three systems of parallel dry cracks was discussed by Piau (1980).

If the host material is anisotropic, general results in the noninteraction approximation are available in 2D (Mauge and Kachanov, 1994). In 3D, the closed-form solutions are known only for fractures confined to the isotropy plane of a transversely isotropic host (Levin and Markov, 2005 and references therein) and to the symmetry planes of a cubic background (Mura, 1987).

The influence of fluid infill of fractures on the overall elasticity was first analyzed by O'Connell and Budiansky (1974) and Budiansky and O'Connell (1976). Their work was restricted to randomly oriented cracks and based on (generally inapplicable to rocks) assumption of identical aspect ratios θ. The latter allowed the authors to retain the conventional crack density e. An arbitrary orientation distribution of fluid-filled cracks with diverse aspect ratios was examined by Shafiro and Kachanov (1997). They introduced the fourth-rank tensor $\boldsymbol{\beta}'$ (equation 29) that properly accounts for the contributions of fractures with different aspect ratios to the overall elasticity.

As the noninteraction approximation was originally thought to be limited to low crack densities, a number of schemes has been proposed to account for crack interactions. This is typically accomplished by putting noninteracting cracks into either an effective matrix or an effective stress field. The self-consistent (O'Connell and Budiansky, 1974) and differential (Vavakin and Salganik, 1975) schemes place the cracks into the effective matrix; the latter does this in increments. Both self-consistent and differential techniques require knowledge of the solution for one crack in the effective matrix; therefore, they are limited to media where such solutions are known, specifically, to random or parallel crack orientations. Another popular scheme was proposed by Mori and Tanaka (1973) and reformulated for cracks by Benveniste (1986). It puts the noninteracting fractures into the average stress field that remains unchanged by the cracks. Perhaps the most advanced extension of the Mori-Tanaka's ideas is called the method of effective field (Levin et al., 2004; Levin and Markov, 2005). This method can account for statistics of the crack positions but does not always yield explicit results.

Geophysics and numerical studies

It appears that many of the above-mentioned results went largely unnoticed by the exploration community, and independent development took place there. Walsh (1965a; 1965b) was the first to examine the effective elastic properties of fractured rocks. Similarly to Bristow (1960), he studied randomly oriented cracks in the noninteraction approximation.

Then two popular noninteraction approximations were proposed by Hudson (1980) and Schoenberg (1980). The critical difference between them is that Hudson (1980) operates in stiffnesses while Schoenberg (1980) operates in compliances. Both theories were originally developed for a single set of cracks embedded in isotropic host rock and later extended to several fracture sets (Hudson 1981; Schoenberg and Muir, 1989; Nichols et al., 1989; Sayers, 2002a; 2002b; Jakobsen et al., 2003) and to anisotropic backgrounds (Schoenberg and Helbig, 1997; Bakulin et al., 2000; Grechka and Tsvankin, 2003; Sayers, 2005). The developments of Hudson (1980) and Schoenberg (1980) and their multiple extensions are not exact; they are essentially the noninteraction approximations augmented by further approximations when the host rock is anisotropic.

Until recently, the accuracy of various effective media schemes remained mostly unknown. The state of affairs has changed after the advances in both computer hardware and software made direct numerical homogenization of the so-called digital rocks feasible (Davis and Knopoff, 1995; Dahm and Becker, 1998; Arns et al., 2002; Saenger and Shapiro, 2002; Saenger et al., 2004; Grechka and Kachanov, 2006a, b; Grechka et al., 2006a, b; Ostoja-Starzewski, 2006). These computational experiments not only elucidated the accuracy of many existing approximations but also extended theoretical knowledge to realistic crack microgeometries that cannot be described analytically.

Finally, there are approaches treating fractures not as compliant inclusions in a stiff matrix but as contacts of rough surfaces (e.g., Yoshioka and Scholz, 1989; Baltazar et al., 2002; Biwa et al., 2005). These approaches define the fracture compliances differently, and perhaps only future measurements on rocks can tell whether the inclusion- or contact-type fracture models are more useful.

REFERENCES

Arns, C. H., M. A. Knackstedt, W. V. Pinczewski, and E. J. Garboczi, 2002, Computation of linear elastic properties from microtomographic images: Methodology and agreement between theory and experiment: Geophysics, **67**, 1396–1405.

Bakulin, A., V. Grechka, and I. Tsvankin, 2000, Estimation of fracture parameters from reflection seismic data, Part I-III: Geophysics, **65**, 1788–1830.

Baltazar, A., S. I. Rokhlin, and C. Pecorari, 2002, On the relationship between ultrasonic and micromechanical properties of contacting rough surfaces: Journal of the Mechanics and Physics of Solids, **50**, 1397–1416.

Benveniste, Y., 1986, On the Mori-Tanaka method in cracked solids: Mechanics Research Communications, **13**, 193–201.

Berg, E., J. Hood, and G. Fryer, 1991, Reduction of the general fracture compliance matrix **Z** to only five independent elements: Geophysical Journal International, **107**, 703–707.

Biwa, S., A. Suzuki, and N. Ohno, 2005, Evaluation of interface wave velocity, reflection coefficients and interfacial stiffnesses of contacting surfaces: Ultrasonics, **43**, 495–502.

Bristow, J. R., 1960, Microcracks and the static and dynamic elastic constants of annealed and heavily cold-worked metals: British Journal of Applied Physics, **11**, 81–85.

Budiansky, B., and R. J. O'Connell, 1976, Elastic moduli of a cracked solid: International Journal of Solids and Structures, **12**, 81–97.

Cardona, R., 2002, Two theories for fluid substitution in porous rocks with aligned cracks: 72nd Annual International Meeting, SEG, Expanded Abstracts, 173–176.

Cheng, C. H., 1993, Crack models for a transversely isotropic medium: Journal of Geophysical Research, **98**, 675–684.

COMSOL Reference Manual, 2005, http://www.comsol.com.

Dahm, T., and T. Becker, 1998, On the elastic and viscous properties of media containing strongly interacting in-plane cracks: Pure and Applied Geophysics, **151**, 1–16.

Davis, P. M., and L. Knopoff, 1995, The elastic modulus of media containing strongly interacting antiplane cracks: Journal of Geophysical Research, **100**, 18 253–18 258.

Eshelby, J. D., 1957, The determination of the elastic field of an ellipsoidal inclusion and related problems: Proceedings of the Royal Society, A241, 376–396.

Grechka, V., 2003, Effective media: A forward modeling view: Geophysics, **68**, 2055–2062.

——— 2005, Penny-shaped fractures revisited: Studia Geophysica et Geodaetica, **49**, 367–383.

Grechka, V., A. Bakulin, and I. Tsvankin, 2003, Seismic characterization of vertical fractures described as general linear-slip interfaces: Geophysical Prospecting, **51**, 117–129.

Grechka, V., P. Contreras, and I. Tsvankin, 2000, Inversion of normal moveout for monoclinic media: Geophysical Prospecting, **48**, 577–602.

Grechka, V., and M. Kachanov, 2006a, Seismic characterization of multiple fracture sets: Does orthotropy suffice? Geophysics, **71**, D93–D105.

———, 2006b, Effective elasticity of rocks with closely spaced and intersecting cracks: Geophysics, **71**, D85–D91.

Grechka, V., and I. Tsvankin, 2003, Feasibility of seismic characterization of multiple fracture sets: Geophysics, **68**, 1399–1407.

Grechka, V., I. Vasconcelos, and M. Kachanov, 2006, The influence of crack shape on the effective elasticity of fractured rocks: Geophysics, **71**, D153–D160.

Gurevich, B., 2003, Elastic properties of saturated porous rocks with aligned

fractures: Journal of Applied Geophysics, **54**, 203–218.
Hill, R., 1963, Elastic properties of reinforced solids; some theoretical principles: Journal of the Mechanics and Physics of Solids, **11**, 357–372.
Hsu, C.-J., and M. Schoenberg, 1993, Elastic waves through a simulated fractured medium: Geophysics, **58**, 964–977.
Hudson, J. A., 1980, Overall properties of a cracked solid: Mathematical Proceedings of Cambridge Philosophical Society, 88, 371–384.
———, 1981, Wave speeds and attenuation of elastic waves in material containing cracks: Geophysical Journal of Royal Astronomical Society, **64**, 133–150.
———, 1991, Overall properties of heterogeneous material: Geophysical Journal International, **107**, 505–511.
Hudson, J. A., E. Liu, and S. Crampin, 1996, The mechanical properties of materials with interconnected cracks and pores: Geophysical Journal International, **124**, 105–112.
Jakobsen, M., J. A. Hudson, and T. A. Johansen, 2003, *T*-matrix approach to shale acoustics: Geophysical Journal International, **154**, 533–558.
Kachanov, M., 1980, Continuum model of medium with cracks: Journal of the Engineering Mechanics Division, ASCE, **106**(EM5), 1039–1051.
———, 1992, Effective elastic properties of cracked solids, Critical review of some basic concepts: Applied Mechanics Review, **45**, 304–335.
———, 1993, Elastic solids with many cracks and related problems, *in* J. W. Hutchinson and T. Wu, eds., Advances in applied mechanics 30: Academic Press Inc, 259–445.
Kachanov, M., and I. Sevostianov, 2005, On quantitative characterization of microstructures and effective properties: International Journal of Solids and Structures, **42**, 309–336.
Kachanov, M., B. Shafiro, and I. Tsukrov, 2003, Handbook of Elasticity Solutions, Kluwer Academic Publishers.
Landau, L. D., and E. M. Lifshitz, 1998, Theory of elasticity, Course of theoretical physics, Vol. 7, 3rd ed.: Butterworth-Heinemann.
Levin, V., and M. Markov, 2005, Elastic properties of inhomogeneous transversely isotropic rocks: International Journal of Solids and Structures, **42**, 393–408.
Levin, V., M. Markov, and S. Kanaun, 2004, Effective field method for seismic properties of cracked rocks: Journal of Geophysical Research, **104**, B08202.
Liu, E., J. A. Hudson, and T. Pointer, 2000, Equivalent medium representation of fractured rock: Journal of Geophysical Research, **105**, 2981–3000.
Markov, K., 1999, Elementary mechanics of heterogeneous media, *in* K. Markov, and L. Preziosi, eds., Heterogeneous media: Micromechanics modeling methods and simulations: Birkhäuser.
Mauge, C., and M. Kachanov, 1994, Effective elastic properties of an anisotropic material with arbitrarily oriented interacting cracks: Journal of Mechanics and Physics of Solids, **42**, 561–584.
Mori, T., and K. Tanaka 1973, Average stress in matrix and average energy of materials with misfitting inclusions: Acta Metallurgica, **21**, 571–574.
Mura, T., 1987, Micromechanics of defects in solids: Martinus Nijhoff Publishers.
Nichols, D., F. Muir, and M. Schoenberg, 1989, Elastic properties of rocks with multiple sets of fractures: 59th Annual International Meeting, SEG, Expanded Abstracts, 471–474.
O'Connell, R. J., and B. Budiansky, 1974, Seismic velocities in dry and saturated cracked solids: Journal of Geophysical Research, **79**, 5412–5426.
Ostoja-Starzewski, M., 2006, Material spatial randomness: From statistical to representative volume element: Probabilistic Engineering Mechanics, **21**, 112–132.
Peacock, S., and J. A. Hudson, 1990, Seismic properties of rocks with distributions of small cracks: Geophysical Journal International, **102**, 471–484.
Piau, M., 1980, Crack-induced anisotropy and scattering in stressed rocks: International Journal of Engineering Sciences, **18**, 549–568.
Rüger, A., 1997, P-wave reflection coefficients for transversely isotropic models with vertical and horizontal axis of symmetry: Geophysics, **62**, 713–722.
Saenger, E. H., O. S. Krüger, and S. A. Shapiro, 2004, Effective elastic properties of randomly fractured soils, 3D numerical experiments: Geophysical Prospecting, **52**, 183–195.
Saenger, E. H., and S. A. Shapiro, 2002, Effective velocities in fractured media, A numerical study using the rotated staggered finite-difference grid: Geophysical Prospecting, **50**, 183–194.
Sayers, C. M., 2002a, Stress-dependent elastic anisotropy of sandstones: Geophysical Prospecting, **50**, 85–95.
———, 2002b, Fluid-dependent shear-wave splitting in fractured media: Geophysical Prospecting, **50**, 393–341.
———, 2005, Seismic anisotropy of shales: Geophysical Prospecting, **53**, 667–676.
Sayers, C. M., and M. Kachanov, 1991, A simple technique for finding effective elastic constants of cracked solids for arbitrary crack orientation statistics: International Journal of Solids and Structures, **27**, 671–680.
Sayers, C. M., and M. Kachanov, 1995, Microcrack-induced elastic wave anisotropy of brittle rocks: Journal of Geophysical Research, **100**, 4149–4156.
Schoenberg, M., 1980, Elastic wave behavior across linear slip interfaces: Journal of Acoustical Society of America, **68**, 1516–1521.
———, 1983, Reflection of elastic waves from periodically stratified media with interfacial slip: Geophysical Prospecting, **31**, 265–292.
———, 2002, Time-dependent anisotropy induced by pore pressure variation in fractured rock: Journal of Seismic Exploration, **11**, 83–105.
Schoenberg, M., and J. Douma, 1988, Elastic wave propagation in media with parallel fractures and aligned cracks: Geophysical Prospecting, **36**, 571–590.
Schoenberg, M., and K. Helbig, 1997, Orthorhombic media, Modeling elastic wave behavior in a vertically fractured earth: Geophysics, **62**, 1954–1974.
Schoenberg, M., and F. Muir, 1989, A calculus for finely layered anisotropic media: Geophysics, **54**, 581–589.
Schoenberg, M., and C. Sayers, 1995, Seismic anisotropy of fractured rock: Geophysics, **60**, 204–211.
Sevostianov, I., and M. Kachanov, 2002, On elastic compliances of irregularly shaped cracks: International Journal of Fracture, **114**, 245–257.
Shafiro, B., and M. Kachanov, 1997, Materials with fluid-filled pores of various shapes: Effective moduli and fluid pressure polarization: International Journal of Solids and Structures, **34**, 3517–3540.
Thomsen, L., 1995, Elastic anisotropy due to aligned cracks in porous rock: Geophysical Prospecting, **43**, 805–829.
Tsvankin, I., 1997, Reflection moveout and parameter estimation for horizontal transverse isotropy: Geophysics, **62**, 614–629.
Vavakin, A. S., and R. L. Salganik, 1975, Effective characteristics of nonhomogeneous media with isolated inhomogeneities, Mechanics of Solids: Allerton Press, 58–66 (English translation of Izvestia AN SSSR, Mekhanika Tverdogo Tela, **10**, 65–75).
Walsh, J. B., 1965a, The effect of cracks on the compressibility of rocks: Journal of Geophysical Research, **70**, 381–389.
———, 1965b, The effect of cracks on uniaxial compression of rocks: Journal of Geophysical Research, **70**, 399–411.
Yoshioka, N., and C. H. Scholz, 1989, Elastic properties of contacting surfaces under normal and shear loads, 1, Theory: Journal of Geophysical Research, **94**, 17,681–17,690.
Zohdi, T. I., and P. Wriggers, 2001, Aspects of the computational testing of the mechanical properties of microheterogeneous material samples: The International Journal of Numerical Methods in Engineering, **50**, 2573–2599.
———, 2005, Introduction to computational micromechanics: Springer.